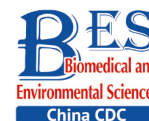


## Original Article



# Evidence on Invasion of Blood, Adipose Tissues, Nervous System and Reproductive System of Mice After a Single Oral Exposure: Nanoplastics versus Microplastics\*

YANG Zuo Sen<sup>1,2</sup>, BAI Ying Long<sup>3</sup>, JIN Cui Hong<sup>4</sup>, NA Jun<sup>1,2</sup>, ZHANG Rui<sup>1,2</sup>, GAO Yuan<sup>1,5</sup>,  
PAN Guo Wei<sup>1,5</sup>, YAN Ling Jun<sup>5,#</sup>, and SUN Wei<sup>1,5,#</sup>

1. Institute of Preventive Medicine, China Medical University, Shenyang 110122, Liaoning, China; 2. Institute of Chronic Diseases, Liaoning Provincial Center for Disease Control and Prevention, Shenyang 110000, Liaoning, China; 3. Department of Maternal and Child Health, School of Public Health, China Medical University, Shenyang 110122, Liaoning, China; 4. Department of Toxicology, School of Public Health, China Medical University, Shenyang 110122, Liaoning, China; 5. Research Center for Universal Health, School of Public Health, China Medical University, Shenyang 110122, Liaoning, China

## Abstract

**Objective** This study was designed to provide the evidences on the toxicokinetics of microplastics (MPs) and nanoplastics (NPs) in the bodies of mammals.

**Methods** 100 nm, 3  $\mu$ m, and 10  $\mu$ m fluorescent polystyrene (PS) beads were administered to mice once by gavage at a dose of 200 mg/kg body weight. The levels and change of fluorescence intensity in samples of blood, subcutaneous fat, perirenal fat, peritesticular fat, cerebrum, cerebellum, testis, and epididymis were measured at 0.5, 1, 2, and 4 h after administration using an IVIS Spectrum small-animal imaging system. Histological examination, confocal laser scanning, and transmission electron microscope were performed to corroborate the findings.

**Results** After confirming fluorescent dye leaching and impact of pH value, increased levels of fluorescence intensity in blood, all adipose tissues examined, cerebrum, cerebellum, and testis were measured in the 100 nm group, but not in the 3 and 10  $\mu$ m groups except in the cerebellum and testis at 4 h for the 3  $\mu$ m PS beads. The presence of PS beads was further corroborated.

**Conclusion** After a single oral exposure, NPs are absorbed rapidly in the blood, accumulate in adipose tissues, and penetrate the blood-brain/testis barriers. As expected, the toxicokinetics of MPs is significantly size-dependent in mammals.

**Key words:** Adipose accumulation; Blood-brain barrier; Blood-testis barrier; Blood uptake; Microplastics; Nanoplastics

Biomed Environ Sci, 2022; 35(11): 1025-1037 doi: 10.3967/bes2022.131

ISSN: 0895-3988

www.besjournal.com (full text)

CN: 11-2816/Q

Copyright ©2022 by China CDC

\*This work was supported by National Natural Science Foundation of China [grand number U21A20399]; Liaoning Revitalization Talents Program [grant number XLYC1802059]; the Key R&D Program of Liaoning Province [grant number 2019JH2/10300044]; and Key Laboratory Program of Liaoning Province [grant number 2018225113]. The funders had no role in study design, data collection and analysis, decision to publish, or preparation of the manuscript.

#Correspondence should be addressed to SUN Wei, Professor, Tel: 86-243-1939406, E-mail: wsun@cmu.edu.cn; YAN Ling Jun, Professor, Tel: 86-243-1939406, E-mail: llyan@cmu.edu.cn

Biographical note of the first author: YANG Zuo Sen, male, born in 1963, MD, majoring in risk assessment of environmental pollution.

## INTRODUCTION

Microplastics (MPs) and nanoplastics (NPs) pollutions have become a growing environmental concern as plastics production has increased to almost 360 million tonnes in 2018<sup>[1]</sup>. MPs pollution had been reported in aquatic habitats from the poles<sup>[2]</sup> to the equator<sup>[3]</sup>. Furthermore, the translocation of MPs particles along food chain has been confirmed<sup>[4,5]</sup>. Indeed, MPs particles have been found not only in seafood<sup>[6,7]</sup>, but also in processed food and beverages, including bottle water, salt, beer, milk, and sugar<sup>[8-11]</sup>. As for NPs ( $\leq 100$  nm in diameter) pollution, it derived from the breaking down of MPs in the environment and some specific industrial or domestic applications such as biomedical products<sup>[12]</sup> and personal care products including toothpastes and cosmetics<sup>[13]</sup>. Unfortunately, NPs had the potential to translocate to a wide variety of organisms<sup>[14]</sup>. All these facts represent a potential dietary exposure pathway to the human body for both MPs and NPs.

According to our knowledge, toxic effects of MPs pollution found in mammals have revealed that MPs pollutants are able to induce gut microbiotadysbiosis<sup>[15,16]</sup>, disturbances in lipid metabolism, oxidative damage, neurotoxicity<sup>[17]</sup> and reproductive disruption<sup>[18]</sup>. Maternal exposure to MPs (0.5  $\mu\text{m}$  and 5  $\mu\text{m}$ ) can even increase the risk of metabolic disorder in their offspring<sup>[19]</sup>. As for NPs, experiments culturing human cerebral and epithelial cells<sup>[20]</sup> and human astrocytoma cells<sup>[21]</sup> have directly showed the oxidative stress and cytotoxic effects of NPs on human cells. In 2017, it was reported that NPs could penetrate the blood-brain barrier in fish and cause behavioral disorders<sup>[22]</sup>. Thereby, NPs are expected to be able to invade the human body more deeply in comparison to MPs. All of these findings suggest that MPs and/or NPs might be a potential threaten to human health. Thus, the European Food Safety Agency attempted to perform a risk assessment of MPs and NPs; however, the assessment could not be completed because the toxicokinetic data are insufficient<sup>[23]</sup>. Thus, the toxicokinetics of MPs and NPs are urgently needed to assess human health risks.

In fact, a study conducted 30 years ago<sup>[24]</sup> reported the absorption of 50 nm – 3  $\mu\text{m}$  polystyrene (PS) beads with covalently-linked fluorescein after 10-day oral exposure. It was concluded that PS particles  $> 300$  nm in size were absent from blood samples and no PS particles (of

any size) were detected in the heart and lungs. In 2019, a 28-day oral feeding study<sup>[25]</sup> focused on micron-size PS (1–10  $\mu\text{m}$ ) and found that only a few particles were present in the intestinal wall. In 2021, NPs were found in mice spleen, lung, kidney, small intestine, large intestine, testis and brain after 28 days oral exposure<sup>[26]</sup>. All of these facts suggested that subacute exposure to MPs and/or NPs resulted in absorption into the blood, but the invasion was size-dependent. With respect to the acute exposure such as a single exposure, studies focusing on the toxicokinetics of MPs and NPs are limited in comparison to common nanomaterials such as silver and  $\text{TiO}_2$ <sup>[27]</sup>. Even if a single exposure might have few practical implications, its foundation role in obtaining basic toxicokinetics index is irreplaceable. The reason for the lack was unknown. The difficulty in tracking skill might be an obstacle performing studies in the related fields. It has been reported that conclusions pertaining to translocation of MPs and NPs drawn from fluorescence were suspected to be artifacts if the stability of the fluorescence label was not confirmed<sup>[28]</sup>. In addition, digestion by gastric acid after oral exposure affected the properties of MPs<sup>[29]</sup>, which increased the complexity in relation to toxicokinetics. So far, the following questions on toxicokinetic data of MPs and NPs in mammals have not been answered: 1) Is there evidence on the uptake in blood for a single oral exposure? 2) Can MPs and NPs accumulate in adipose tissues due to lipophilicity? 3) Are MPs and NPs able to penetrate the blood-brain and blood-testis barriers in mammals as observed in fish?

The present study was designed to clarify the characteristics and differences in the absorption of MPs and NPs into the bodies of mammals after acute oral exposure. 100 nm, 3  $\mu\text{m}$  and 10  $\mu\text{m}$  PS beads with fluorescent dyes incorporated into the polymer matrix were fed by gavage once to male Kunming strain mice. The absorption level of MPs and NPs and the time-dependent characteristics in blood, various adipose tissues, the nervous system, and the reproductive system were measured by an IVIS Spectrum small-animal imaging system for 4 h. The observations were further proved by confocal laser scanning, histological examination, and transmission electron microscope. We believe that our findings will reveal the different absorption, distribution *in vivo*, and penetrating ability between MPs and NPs, and provide pilot evidence for toxicokinetics of MPs and NPs in mammals after confirming the leaching of fluorescence label and the impact of pH value

imitating the condition in stomach.

## MATERIAL AND METHODS

### *Micro- and nano-PS Beads*

100 nm (Cat. No. G100), 3  $\mu\text{m}$  (Cat. No. G0300B), and 10  $\mu\text{m}$  (Cat. No. G1000B) diameters of PS fluorescent beads (Fluoro-Max<sup>TM</sup> Green Fluorescent Polymer Microspheres) were purchased from Thermo Fisher Scientific Corporation, USA. Those particles are internally dyed using proprietary Firefli fluorescent process and coupled with a dye-free surface in order to prevent dye leaching. The beads are packaged in deionized water with trace amounts of surfactant. The excitation spectrum was 488 nm and emission spectrum was 508 nm. The concentration of those fluorescent PS beads is 1% solids by weight which represents  $1.8 \times 10^{16}$  particles  $\text{L}^{-1}$  for 100 nm beads,  $7.5 \times 10^{11}$  particles  $\text{L}^{-1}$  for 3  $\mu\text{m}$  beads, and  $1.9 \times 10^{10}$  particles  $\text{L}^{-1}$  for 10  $\mu\text{m}$  beads, respectively. They were stored at 4 °C in the dark and reversed gently before use.

### *Animals*

Forty-eight male Kunming strain mice ( $20 \pm 1$  g) were purchased from Beijing HFK Bioscience Co., LTD (license number: 1103221911010176; Beijing China). All animals were acclimated under specific pathogen-free conditions for 1 week before starting the experiments. Animals were maintained in the Laboratory Animal Center of China Medical University at a room temperature of  $23 \pm 2$  °C, a relative humidity of 45%–60% and a 12-h light/dark cycle. All mice were given free access to food and water, but fasted for 12 h before exposure. The experimental protocol was approved by the Ethical Requirements of Experimental Animals of China Medical University (Number: CMU2019216).

### *Experimental Design*

With respect to acute oral exposure dose, a study with 28 days of feeding<sup>[25]</sup> did not show a considerable health risk to mice. Thus, we decided to select the upper limit of the dose range proposed for fluorescence imaging [20 to 200  $\text{mg} \cdot \text{kg}^{-1} \cdot \text{body weight (BW)}$ ]<sup>[30]</sup> as a single gavage dose in the current study. In our study, 400  $\mu\text{L}$  suspension (1% solid by weight) was used to achieve 200  $\text{mg} \cdot \text{kg}^{-1}$  BW for the mice of average 20 g-BW.

With respect to particle size, a 100 nm diameter is the biggest size for NPs and was selected as an indicator of NPs. We initially focused on 2.5  $\mu\text{m}$

referring to fine particulate matter ( $\text{PM}_{2.5}$ ) and a larger representative for MPs. Because 3  $\mu\text{m}$  is the closest size to 2.5  $\mu\text{m}$  among all tradable commodities and 10  $\mu\text{m}$  tends to be distinguishable from 3  $\mu\text{m}$ , the characteristics of these two sizes of MPs were explored and compared with NPs.

Mice were randomly divided into the following four groups: 0.9% normal saline control ( $n = 12$ ), 100 nm PS fluorescent beads ( $n = 12$ ), 3  $\mu\text{m}$  PS fluorescent beads ( $n = 12$ ) and 10  $\mu\text{m}$  PS fluorescent beads ( $n = 12$ ). All mice were fasted for 12 h and 400  $\mu\text{L}$  PS beads (100 nm:  $7.2 \times 10^{12}$  particles; 3  $\mu\text{m}$ :  $3.0 \times 10^8$  particles; 10  $\mu\text{m}$ :  $7.6 \times 10^6$  particles) were administered once by gavage. In the control group, mice were given the same volume of saline solution by the same route. Three mice from each group were sacrificed 0.5, 1, 2, and 4 h after gavage<sup>[31,32]</sup>. The administration time was determined according to the evaluation of nanoparticles using fluorescence imaging<sup>[30]</sup>. Blood was collected as much as possible after eyeball extraction. Mice were euthanized by cervical dislocation and tissues samples, including the subcutaneous fat, perirenal fat, peritesticular fat, cerebrum, cerebellum, testis, and epididymis were obtained and weighed for further measurements.

### *Fluorescence Imaging*

An IVIS Spectrum small-animal imaging system (IVIS Spectrum, PerkinElmer Inc, US) was used to measure fluorescence intensity of tissues to indicate the PS content ( $\lambda_{\text{Ex}}$  505 nm,  $\lambda_{\text{Em}}$  515 nm). The same tissues from PS-treated and control groups were placed on one black paper and imaged at the same time. 100  $\mu\text{L}$  of blood was taken to measure the fluorescence intensity with the same method as solid tissues. Entire tissues were selected as the region of interest for fluorescence analysis. The total radiant efficiency units from selected area were used to indicate the fluorescence intensity. Radiant efficiency was corrected for tissue weight (g) and volume (mL) in all calculations<sup>[31]</sup>. The fold increase of fluorescence intensity (fold = total radiant efficiency of tissue in exposure group/mean radiant efficiency of tissue in the control group) was calculated to indicate the change in strength. As for the blood, the fluidity of liquid resulted in the variation of radiant area ( $\text{cm}^2$ ) even for the same volume. Thus, radiant area was further corrected while calculating fold increase.

### *Histological Examination*

Solid tissues with significant fluorescent imaging were performed histological examination to

corroborate the findings by IVIS Spectrum. Samples were immersed in fixative immediately after fluorescent imaging for at least 24 h. Dehydration and paraffin infiltration were conducted by putting sample in 75%–100% alcohol, xylene and paraffin for appropriate time. Embedding was undertaken through processing tissue sample in melted paraffin in cassettes. The embedded samples were frozen at  $-20^{\circ}\text{C}$  until paraffin solidify completely. Paraffin block was taken out and trimmed accordingly. Four  $\mu\text{m}$  sections were cut and treated by hematoxylin-eosin (HE) staining and DAPI dye, respectively.

### **Confocal Laser Scanning Microscope**

For the blood sample, confocal laser scanning was conducted to confirm the presence of PS beads in blood even if the absorption was not found by IVIS Spectrum due to its detection limit. Ten  $\mu\text{L}$  blood sample was further examined ( $\lambda_{\text{Ex}}$  488 nm,  $\lambda_{\text{Em}}$  500–550 nm) using Nikon A1-R (Japan) confocal laser scanning microscope (CLSM). In this study, a visual magnification of  $600\times$  (a  $10\times$  ocular and  $60\times$  objective) was used for all CLSM examination.

### **Transmission Electron Microscope**

The presence of PS beads in blood sample was further proved by transmission electron microscope (TEM, 200kV, JEM-2100F, JEOL) because it can achieve the highest image quality even for the particle with a size under 0.5 nm. Blood sample was added to an equal volume of hydrogen peroxide 30% and put in a  $50^{\circ}\text{C}$  water bath until it became colorless. TEM examination was performed to enhance the evidence, especially for NPs.

### **Confirmation on the Leaching of Fluorescent Dye**

The leaching of fluorescent dye was examined, especially for NPs. Two experiments were performed. The first experiment was performed by using the method reported by Schür et al.<sup>[28]</sup> which focused on NPs: 127  $\mu\text{m}$  thick medical grade silicone rubber was placed in particle suspensions for 24 h, rinsed in ultrapure water after the incubation, and imaged by CLSM. There were three groups according to the dispersion status before incubation: 1) 0.9% normal saline control; 2) dispersing 100 nm PS suspension by reversing gently as conducted in this study; and 3) dispersing 100 nm PS suspension by sonicating for 30 min.

The second experiment was performed by TEM examination to further identify 100 nm and 3  $\mu\text{m}$  PS hydrochloric acidbeads status after different dispersing methods. The numbers of PS beads with

different sizes were counted for three view fields of each condition.

### **Impact of pH Value on MPs**

Low pH condition was reported to modulate the properties of MPs<sup>[29]</sup>. The pH value in stomach of mice is in the range of 2.98 to 4.04<sup>[33]</sup>. With respect to 100 nm PS, the incubation of 24 h and dry overnight were needed for CLSM and TEM examinations. Thus, neutralization at 0.5, 1, 2, and 4 h was necessary. However, the dose changes and the impact of alkali made it difficult to make conclusion. Thus, only the impact of low pH on 3  $\mu\text{m}$  PS beads was performed. The 3  $\mu\text{m}$  PS beads were added to the solution with a pH of 2.61 in a 1:1 volume ratio. The status of 3  $\mu\text{m}$  PS beads was examined by CLSM at 0, 0.5, 1, 2, and 4 h. In addition, the original status of both 100 nm and 3  $\mu\text{m}$  PS beads were observed by TEM.

### **Quality Control**

All surgical instruments were cleaned using ultrapure water and sterilized thoroughly before dissection. The tissues were thrice-rinsed with 0.9% normal saline to avoid cross-contamination from blood and dried on filter paper. All tubes, filter papers, saline solutions, and black papers used were detected by the IVIS Spectrum to assure the avoidance of fluorescence contamination. Also, the food and feeding water were measured, even if animals were fasted for 12 h. The imaging results showed that feeding water was free of fluorescence, but the food contained a strong fluorescence signal (Supplementary Figure S1 available in [www.besjournal.com](http://www.besjournal.com)).

### **Statistical Analysis**

Data are expressed as the mean  $\pm$  standard deviation (SD). Fluorescence intensity and fold-increase values were analyzed separately. The differences among time points were analyzed using one-way analysis of variance followed by the Least Significant Difference test for multiple comparisons. A  $P < 0.05$  was considered significant. SPSS 13.0 software (SPSS Co., Ltd., Chicago, IL, USA) was used to perform data analysis.

## **RESULTS**

### **Autofluorescence Intensity of Various Tissues at different Time Points by IVIS Spectrum**

Mice in the control group were given saline



solution by gavage. IVIS Spectrum imaging showed that the levels of autofluorescence intensity differed among the tissues (Table 1). Blood had the lowest autofluorescent signal. By comparison, epididymis had the highest autofluorescence intensity (123 times that of blood). Due to the autofluorescence, the fold increase (PS-treated group vs. control group) was used to indicate the change in strength. Because no significant differences existed among the different time points for each tissue in the control group, mean value of different time points was calculated as mean radiant efficiency of tissue in the control group to increase the stability of the autofluorescence intensity.

#### **The Absorption of 100 nm, 3 $\mu$ m, and 10 $\mu$ m PS Beads in Blood by IVIS Spectrum**

Figure 1A shows the time course changes of fluorescence intensity in blood after administering PS beads by gavage at a dose of 200 mg·kg<sup>-1</sup>·BW. In the 100 nm PS exposure group, the fluorescence intensity increased significantly at 0.5, 1, and 2 h ( $P < 0.05$ ) in comparison to the control group; the highest level was at  $t = 0.5$  h. Up to 4 h, the fluorescence intensity decreased to the same level as the control group and was significantly lower than level at 0.5 h ( $P < 0.05$ ). By contrast, no changes were observed for 3 and 10  $\mu$ m PS exposure.

#### **Distribution of 100 nm, 3 $\mu$ m, and 10 $\mu$ m PS Beads in Adipose Tissue by IVIS Spectrum**

For all adipose tissues examined, the increases in fluorescence intensity in the 100 nm PS-treated group were significant, even at the first time point ( $P < 0.05$ ). However, the change trend was different among different adipose tissues. For subcutaneous and perirenal fat, fluorescence

intensity continued to increase for 2 h ( $P < 0.05$ ) after exposure, then decreased significantly at 4 h, but was still at a significantly high level in comparison to the control group ( $P < 0.05$ ). The highest increasing level of fluorescence intensity was 3.65 times and 5.63 times as the control group, respectively. For peritesticular fat, the fluorescence intensity continued to increase during the entire time period ( $P < 0.05$ ). At the 4 h time point, fluorescence intensity reached the highest level (4.41 times). In contrast, there were no significant changes observed in the 3 and 10  $\mu$ m PS-treated groups (Figure 1B and Supplementary Figure S2-1A1–C3, available in [www.besjournal.com](http://www.besjournal.com)).

#### **Distribution of 100 nm, 3 $\mu$ m, and 10 $\mu$ m PS Beads in the Nervous System by IVIS Spectrum**

Cerebrum and cerebellum samples were detected by IVIS Spectrum. The results could reflect the ability of micro- and nano- PS beads to penetrate the blood-brain barrier. Figure 1C shows the time course changes of fluorescence intensity in the nervous system at different time points after PS beads exposure. After gavage at a dose of 200 mg·kg<sup>-1</sup>·BW, the fluorescence intensity of the cerebrum increased significantly at all time points ( $P < 0.05$ ) in the 100 nm PS-treated group. With respect to the cerebellum, a significant increase in fluorescence intensity was also observed since the 1 h time point ( $P < 0.05$ ). In the 3  $\mu$ m PS-treated group, a significant increase in fluorescence intensity (1.54 times) was observed in the cerebellum 4 h after oral exposure ( $P < 0.05$ ). In the 10  $\mu$ m PS-treated group, no change was observed. The IVIS Spectrum small-animal imaging system images are shown in Supplementary Figure S2-2D1–E3.

**Table 1.** Autofluorescence intensity of tissues in control group at different time points (unit: [(p/sec)/( $\mu$ W/cm<sup>2</sup>)]/g,  $1.00 \times 10^8$ )

Tissues	Mean $\pm$ SD				
	0.5 h ( $n = 3$ )	1 h ( $n = 3$ )	2 h ( $n = 3$ )	4 h ( $n = 3$ )	Total
Epididymis	138.0 $\pm$ 91.5	106.0 $\pm$ 21.5	97.2 $\pm$ 14.7	81.9 $\pm$ 10.40	106.0 $\pm$ 46.1
Subcutaneous fat	93.4 $\pm$ 27.8	83.3 $\pm$ 15.8	64.0 $\pm$ 14.4	70.1 $\pm$ 16.3	77.7 $\pm$ 20.4
Testis	62.1 $\pm$ 10.1	69.4 $\pm$ 2.5	61.4 $\pm$ 4.9	70.2 $\pm$ 11.7	65.8 $\pm$ 8.16
Perirenal fat	47.6 $\pm$ 28.7	48.0 $\pm$ 19.2	44.9 $\pm$ 13.7	44.8 $\pm$ 16.0	46.3 $\pm$ 17.3
Peritesticular fat	39.4 $\pm$ 3.4	46.8 $\pm$ 24.9	50.2 $\pm$ 12.5	41.9 $\pm$ 12.8	44.6 $\pm$ 13.9
Cerebellum	16.7 $\pm$ 2.6	16.8 $\pm$ 2.5	21.8 $\pm$ 0.8	16.9 $\pm$ 2.8	18.1 $\pm$ 3.0
Cerebrum	18.0 $\pm$ 0.70	18.4 $\pm$ 0.4	17.3 $\pm$ 3.34	17.64 $\pm$ 3.4	17.8 $\pm$ 2.1
Blood*	0.97 $\pm$ 0.28	0.78 $\pm$ 0.24	0.88 $\pm$ 0.03	0.78 $\pm$ 0.03	0.86 $\pm$ 0.18

**Note.** \* Adjusted by volume (mL).

### Distribution of 100 nm, 3 $\mu$ m, and 10 $\mu$ m PS beads in the reproductive system by IVIS Spectrum

Figure 1D shows the time course changes of fluorescence intensity in the reproductive system at different time points after PS beads exposure. In the testis, the increase in fluorescence intensity at 4 h was significant (fold = 1.19,  $P < 0.05$ ) in the 100 nm PS-treated group; however, no significance existed in the epididymis even if the level reached a 1.22 fold increase. Interestingly, the autofluorescence intensity of the epididymis was nearly 2 times the level of the testis. In the 3  $\mu$ m PS-treated group, a significant increase in fluorescence intensity also reached statistical significance ( $P = 0.047$ ). No significant changes were demonstrated for the 10  $\mu$ m PS beads. The images in IVIS Spectrum are shown in Supplementary Figure S2-F1–G3.

### CLSM and TEM Corroborations for the Presence of PS Beads in Blood

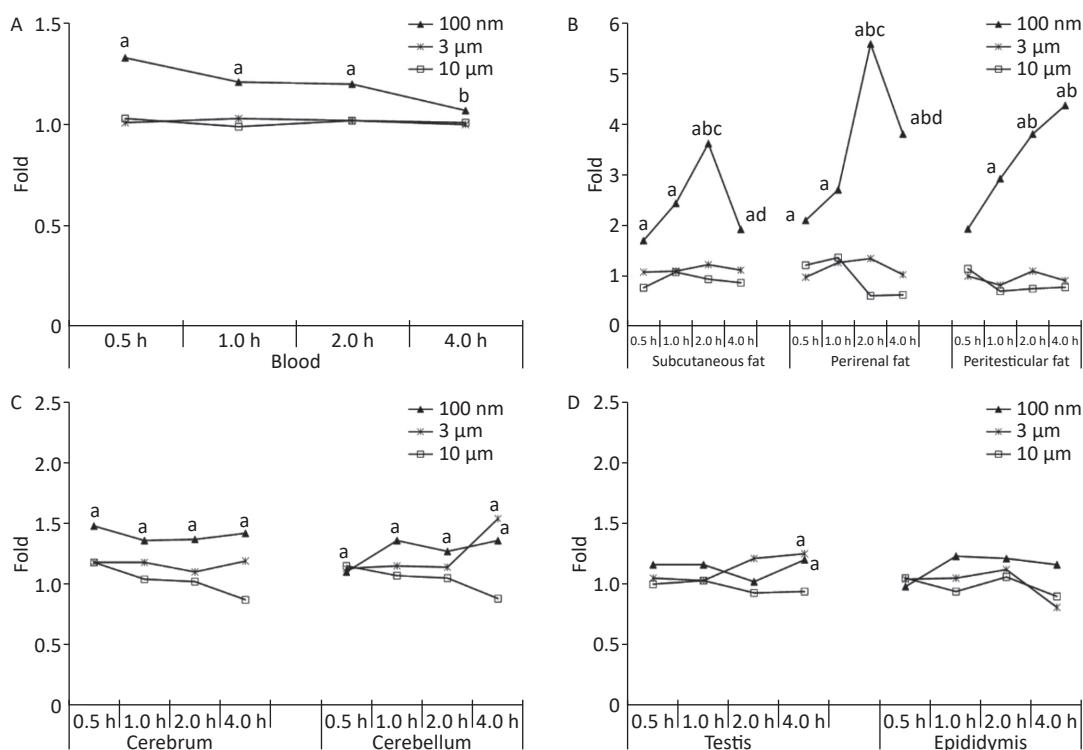
In this study, the absorption of PS beads in blood was confirmed by CLSM and results are shown in

Figure 2. Since IVIS Spectrum revealed that blood sample at 0.5 h have the strongest fluorescent intensity in the 100 nm PS-treated group, the blood samples at 0.5 h was further examined by CLSM. Even if green PS beads was found (Figure 2C–D), it was difficult to pinpoint the exact location in blood stream due to its small size. As for the 3  $\mu$ m PS-treated group, the blood samples were also examined by CLSM because significant increase were found in cerebrum and testis by IVIS spectrum at 4 h after exposure. Interesting, the presence of PS bead was found since 2 h after exposure (Figure 2E–F). No any green fluorescence beads was found in saline control group (Figure 2A–B).

Examination by TEM was also performed because the CLSM is not enough to distinguish the nanoparticle from fluorescent dye. Particles with diameter around 100 nm and 3  $\mu$ m were found (Figure 2G–H).

### Histological Corroboration

For solid samples, histopathology examination was conducted to confirm the significant findings



**Figure 1.** Time course changes of fluorescence intensity in blood, adipose tissues, nervous system, and reproductive system after administering PS beads by gavage at a dose of 200 mg·kg<sup>-1</sup>·BW.  $n = 3$ ; (A) blood; (B) adipose tissues; (C) nervous system; (D) reproductive system. a, compared with control,  $P < 0.05$ ; b, compared with 0.5 h,  $P < 0.05$ ; c, compared with 1 h,  $P < 0.05$ ; d, compared with 2 h,  $P < 0.05$ . PS, polystyrene.

revealed by IVIS spectrum. Thus, samples of subcutaneous fat, perirenal fat, peritesticular fat, cerebrum, cerebellum, and testis at 4 h in 100 nm PS treated group and samples of cerebellum and testis at 4 h in 3  $\mu$ m PS-treated group were examined. Among all adipose tissues in 100 nm PS-treated group, fluorescence signals were brighter in adipose cells except lipid droplet (Figure 3). In the cerebrum, brighter fluorescence signals were found in blood vessels, perivascular space and nerve cells in cortex in 100 nm PS-treated group (Figure 4A2–A4). Furthermore, nerve cells tended to be hyperchromatic nuclei, pyknotic and irregular. Histological results of the cerebellum are shown in Figure 4C1–E4. The fluorescence signals were observed through the whole granular layer in 100 nm PS-treated group. The stronger signals in medulla were also found in 3  $\mu$ m PS-treated group. Histological results of testis are shown in Figure 4F1–H4). The brighter fluorescence signals were found in the connective tissues and leydig cells, not the seminiferous tubule, in both 100 nm and 3  $\mu$ m PS-treated groups. However, the thinner seminiferous tubule with reduced spermatogenic cell layers was observed in comparison to control group and the histopathological changes tended to be serious in 3  $\mu$ m PS-treated group.

### Fluorescent Dye Leaching Experiment

The results of leaching experiment examined by CLSM are shown in Figure 5. Different dispersing condition before exposure were revealed to directly affect the leaching. After dispersing PS suspensions by sonicating for 30 min as reported by Schür C et al.<sup>[28]</sup>, the strong fluorescent signal pertaining to leaching was also observed (Figure 5E–F). In contrast, after dispersing PS suspensions by reversing gently as conducted in this study, the leaching was not observed except the residual particles that was not washed off and adhered to the silicone rubber strip, especially the edges (Figure 5C–D).

The confirmation was further conducted through TEM. Comparing between different dispersing conditions, the number of particles with smaller size observed frequently in group of sonicating for 30 min (Supplementary Figure S3B available in [www.besjournal.com](http://www.besjournal.com)). Furthermore, the numbers of particles with diameter of > 80 nm, 50–80 nm and < 50 nm were counted for 3 view-fields in each group. The percentages of size > 80 nm in reversing gently group and sonicating for 30 min group were 92.3% and 65.6%; whereas the rates of size < 50 nm were 0 and 8.6% respectively.

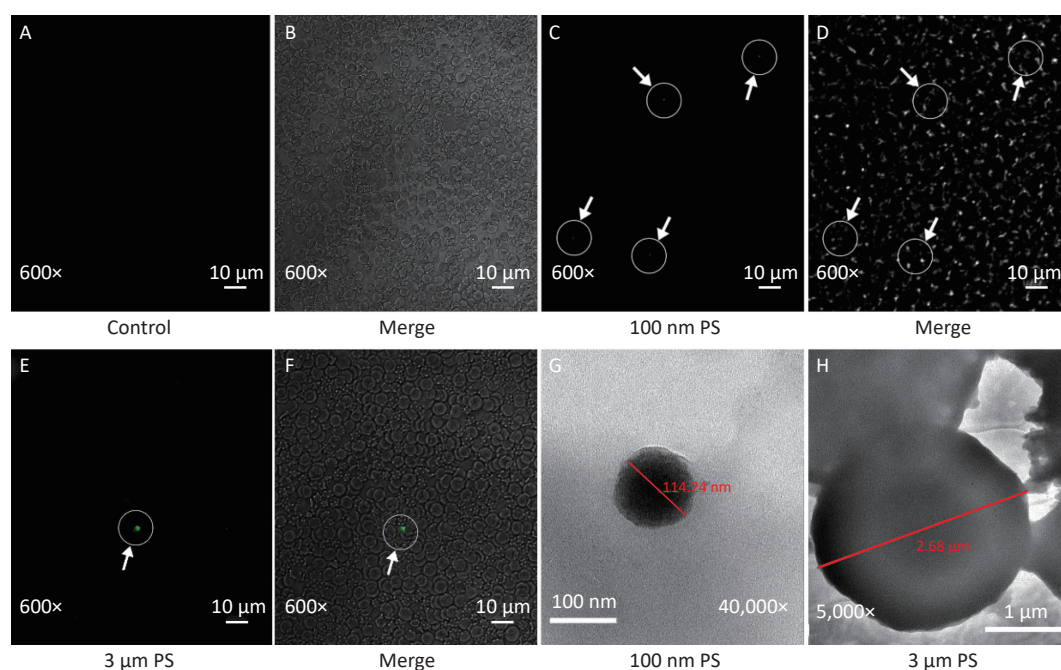


**Figure 2.** The evidence of PS beads in blood samples examined by CLSM and TEM. (A–B) are the fluorescence and bright-field images in the control group (600 $\times$ ). (C–D) are the images in 100 nm PS-treated group (600 $\times$ ). (E–F) are the images in 3  $\mu$ m PS-treated group (600 $\times$ ). (G) (40,000 $\times$ ) is the TEM image for 100 nm PS bead. (H) (5,000 $\times$ ) is the TEM image for 3  $\mu$ m PS bead. PS, polystyrene.

### Impact of pH value on MPs

The results pertaining to the impact of pH on the properties of 3  $\mu\text{m}$  PS beads are shown in Figure 6. CLSM examination revealed that there were no changes occurred to 3  $\mu\text{m}$  PS beads before and after adding to the solution with a pH of 2.61, even for 4 h (Figure 6E), which indicated that low pH level was unable to affect MPs. The structures of 100 nm and 3  $\mu\text{m}$  PS beads were observed by TEM (Figure 6F–G). For the 100 nm PS beads (95.37 nm), the thickness of dye-free surface was around 10 nm. In contrast, the thickness of dye-free surface was about 400 nm for

3  $\mu\text{m}$  PS beads (2.60  $\mu\text{m}$ ).

### DISCUSSION

The present study was conducted using a single oral exposure to micro- and nano- PS beads. Firstly, we examined the leaching of fluorescence before exposing PS beads to mice. Our results confirmed that dispersing condition could be the cause of leaching. Sonicating for 30 min did lead to the leaching of fluorescent dye, same as reported by Schür C et al.<sup>[28]</sup>. In contrast, the dispersing method used in this study did not make the leaching happen.

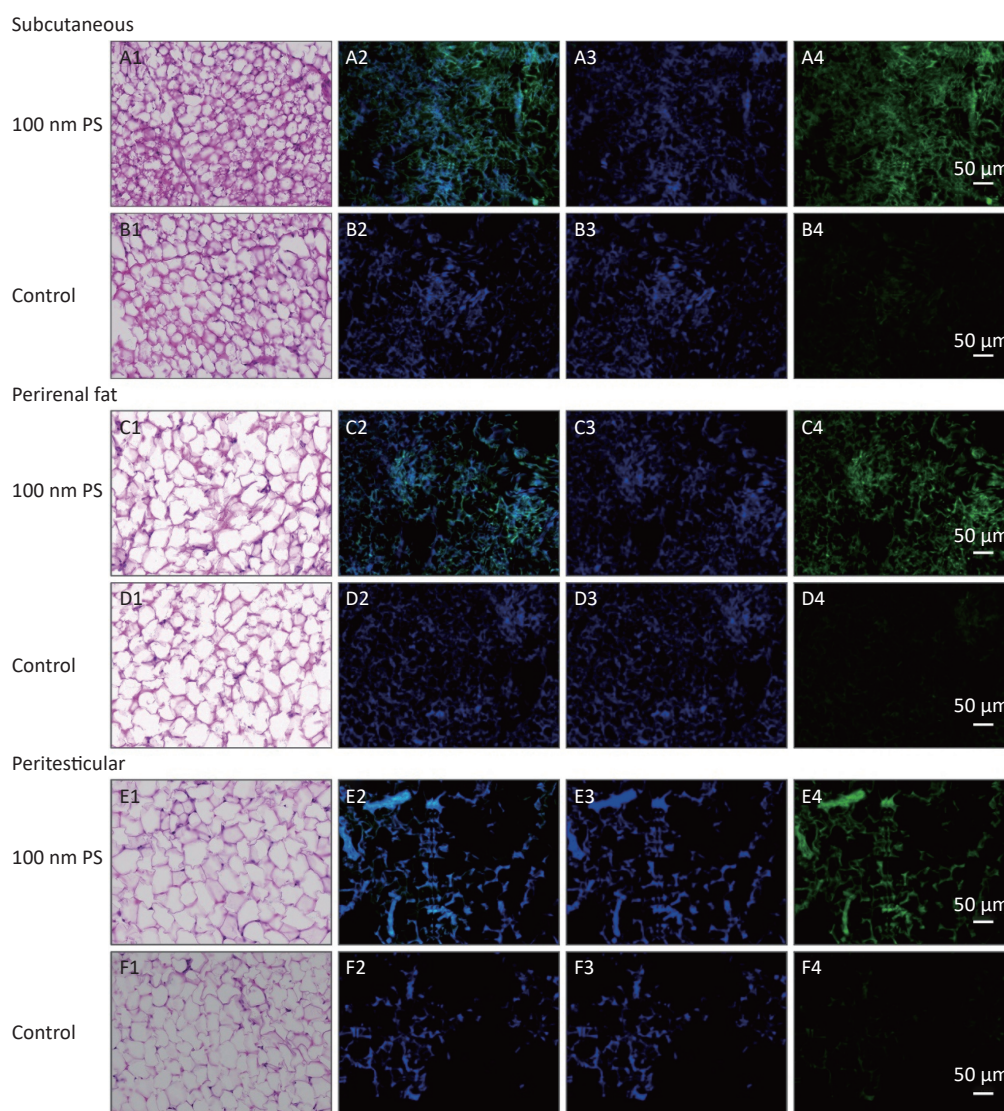


**Figure 3.** Histological examination of adipose tissues (200 $\times$ ). The first column is the image of HE staining. The second is the merge of both PS fluorescence and DAPI dye. The third is the fluorescence image of DAPI dye. The fourth is the fluorescence image of PS beads (green). PS, polystyrene. DAPI, 4',6-diaminidene-2-phenylindole.



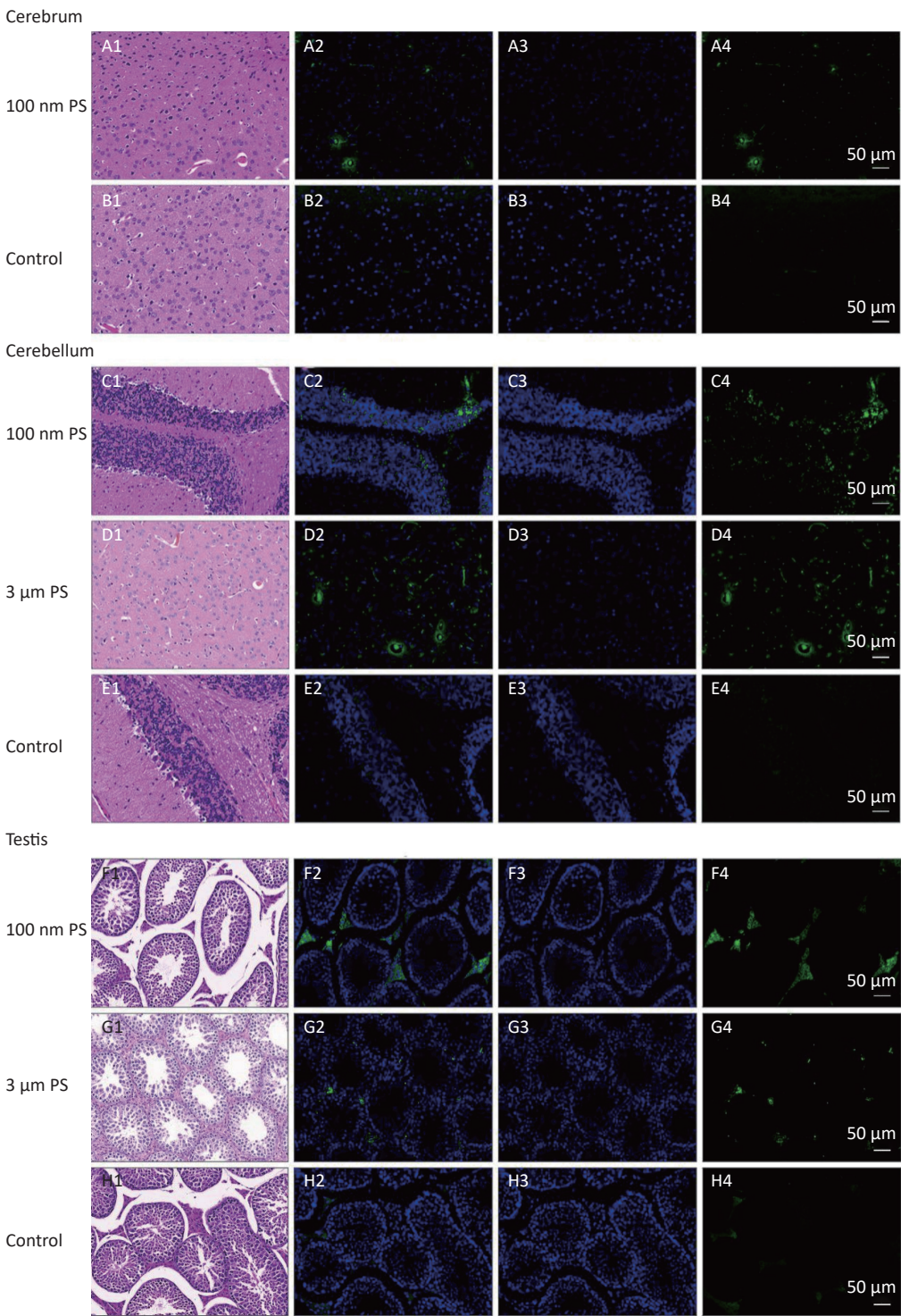


**Figure 4.** Histological results of the cerebrum tissues, cerebellum tissues and testis tissues (200×). The first column is the image of HE staining. The second is the merge of both PS fluorescence and DAPI dye. The third is the fluorescence image of DAPI dye. The fourth is the fluorescence image of PS beads (green). PS, polystyrene. DAPI, 4',6-diaminidide-2-phenylindole.



With respect to the impact of low pH (2.98–4.04) in stomach of mice<sup>[33]</sup>, our findings indicated that pH value as low as 2.61 could not affect MPs. It might be

due to the stable properties of PS or the thick surface of PS beads to resist the destruction of acid. Even if we were unable to exclude the impact of low

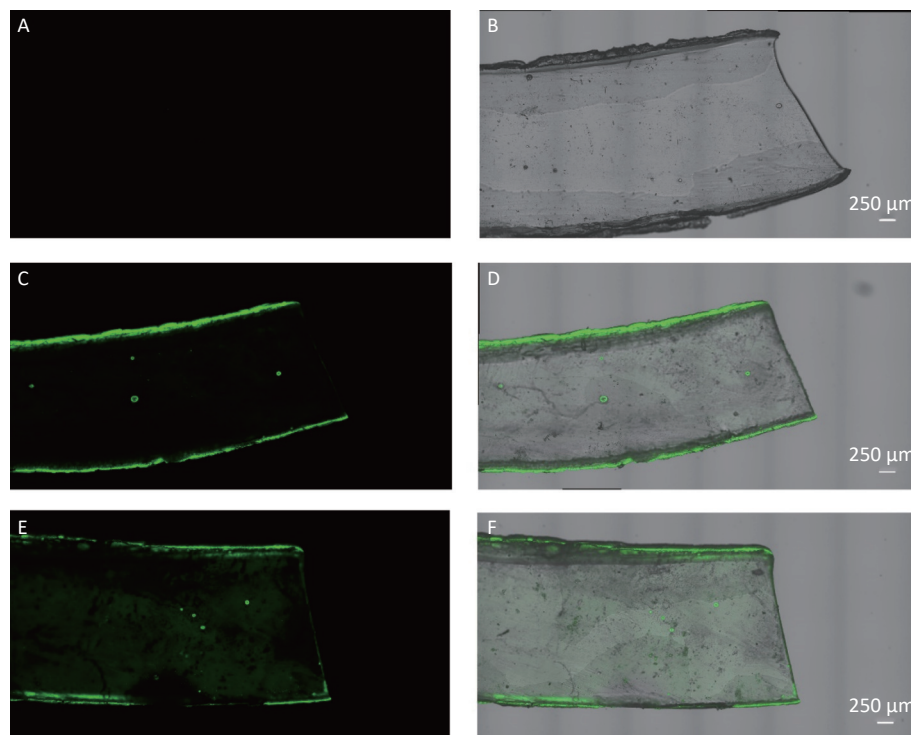


**Figure 5.** The leaching examination by confocal laser scanning microscope (100×). (A–B) are the fluorescence image and merged image (fluorescence and bright-field) of silicone rubber strip in 0.9% normal saline control group. (C–D) are the images in dispersing condition of reversing gently group. (E–F) are the images in dispersing condition of sonicating for 30 min group.

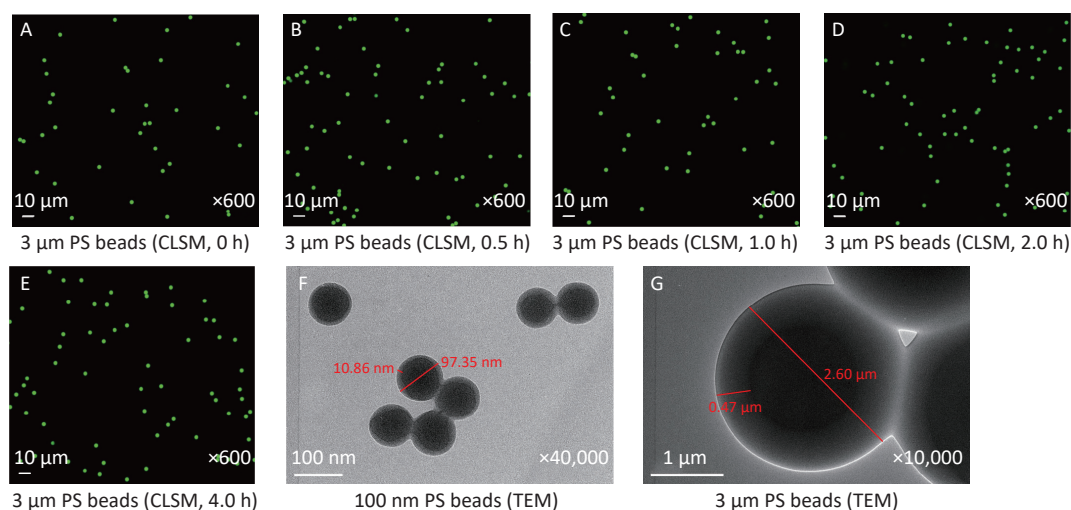


**Figure 6.** CLSM examination for the impact of pH on 3  $\mu$ m PS beads and TEM observation on 100 nm and 3  $\mu$ m PS beads. (A) is the image before adding acid solution (600×). (B–E) are the images of 3  $\mu$ m PS beads at 0.5, 1, 2, and 4 h after adding the equal volume of solution with a pH of 2.61 (600×). (F–G) are the TEM images of 100 nm (40,000×) and 3  $\mu$ m (10,000×) PS beads. PS, polystyrene. .

pH on NPs that had 40 times thinner surface than MPs, the presences of 100 nm PS beads in the blood were found by TEM. After controlling for contamination the fluorescence leaching, our findings revealed that NPs were rapidly absorbed in blood and accumulated in adipose tissue after acute and high dose oral exposure. Moreover, NPs, even the largest size of 100 nm, had the ability to penetrate the blood-brain and blood-testis barriers. Thus, the toxicity of NPs should be the focus of attention to prevent the potential risk to human health. In contrast, the 3  $\mu$ m MPs could enter the blood and penetrate both barriers, but was unable to be absorbed into adipose tissues. No absorption evidence was shown for 10  $\mu$ m MPs.

With respect to the uptake of NPs and MPs in blood, the results in this study indicated that a single oral exposure to NPs could lead to rapid uptake. Among the time points observed, the fluorescence intensity was the highest at 30 min, then decreased, which indicated that NPs were absorbed rapidly. This finding was corroborated by CLSM and TEM even if the numbers of PS beads was found to be particularly few. Together these facts indicated that NPs could be absorbed into blood and rapidly disappeared for tissue distribution, which is the same as silver nanoparticles<sup>[34]</sup>. Interestingly, we did not find any absorption evidence in blood for both 3  $\mu$ m and 10  $\mu$ m by IVIS Spectrum. This result seemed to be in agreement with the conclusion drawn from chronic oral exposure<sup>[24]</sup>, i.e., PS particles > 300 nm were not absorbed into blood. However, the presences of 3  $\mu$ m PS beads in blood were found by both CLSM and TEM. The absence of MPs in blood by IVIS Spectrum might be due to the detection limits. In this study, the number of 3  $\mu$ m PS particles was 24,000 times lower than that of 100 nm PS particles; whereas its size was much bigger. Thus, the absorption of 3  $\mu$ m MPs was expected to be fewer and slower than the NPs. Since the fluorescent intensity of 100 nm PS in blood sample was already in a particularly low level in IVIS Spectrum examination, the fluorescent intensity 3  $\mu$ m PS tended to be much lower, even lower than the detection limits. As for the assessment of hematological toxicity, we initially focused on the time-dependent characteristics of toxicokinetics and only the presence of PS beads in blood was proved. We did not count the numbers of white blood cells or red blood cells as the report on pesticide<sup>[35]</sup>. Further studies focusing on toxicity of MPs and NPs should be conducted to achieve this aim.

With respect to accumulation in adipose tissues,

our study revealed this change in all adipose tissues examined, but only for NPs and not for any size of MPs. Histological examination further corroborated those findings. Interestingly, even if their autofluorescence intensities were in a higher level, especially subcutaneous fat, among tissues measured in this study, the fold increases were also the highest. Thus, the absolute doses of nano-PS distributed in those adipose tissues were expected to be the highest after gavage. This fact suggested that the adipose tissues could be a target organ accumulating most NPs after a single oral exposure. It might due to the high lipophilicity of plastic particles<sup>[36]</sup>. Since the accumulation in peritesticular fat was still continual up to the end of observation period (4 h), the time course of accumulation characteristics should be studied with a longer observation period. By contrast, the decreasing of fluorescence intensities in subcutaneous fat and perirenal fat were found 4 h after exposure. The migration to other tissues might be the reason because of the observations of NPs in other tissues after oral exposure<sup>[26]</sup>. The NPs might accumulate firstly in adipose tissues due to the lipophilicity and then migrate. In addition, the presence of NPs in kidney<sup>[26]</sup> increased the likelihood that NPs could be eliminated through urine. However, the evidence has not yet been found up to now. Because a disturbance of plastic particles on lipid metabolism has been reported<sup>[17]</sup>, whether adipose tissue is the storage organ only or the target organ also needs to be clarified.

In the terms of penetrating ability, NPs have been shown to penetrate the blood-brain barrier in fish<sup>[22]</sup>. Recently, the presence of NPs in mice brain was also found for 28 days exposure<sup>[26]</sup>. Our findings indicated that NPs can penetrate the blood-brain barrier in mice, even after a single oral exposure to the largest size of NPs. Both the cerebrum and cerebellum were confirmed by histological examination that NPs were able to enter nerve cells. Especially in the cerebrum, the significance was observed during the entire observation period and the histopathological changes were found. In addition to the blood-brain barrier, NPs can also penetrate the blood-testis barrier due to the significant increase in testis. In the epididymis, although the increase did not reach significance, it was still considerable because the autofluorescence intensity of the epididymis was the highest among all measured tissues. Under the same fold-increase, the absolute increase in fluorescence intensity of the epididymis was nearly 2 times and over 5 times the

amount in the testis and nervous system, respectively. Besides, the penetrating abilities were also found for 3  $\mu\text{m}$  PS beads 4 h after exposure. The evidences of both IVIS Spectrum and histology were obtained from the cerebellum and the testis. From the view point of histopathological changes, effects of 3  $\mu\text{m}$  PS beads on testis tended to be more obvious than 100 nm PS beads. Although the sperm quality<sup>[37]</sup> was not examined in this toxicokinetics design, the changes of seminiferous tubule did be found. This finding could be another evidence confirming the penetrating ability. As for 10  $\mu\text{m}$  MPs, we did not find any evidence in relation to penetrating ability. However, the conclusion should be drawn cautiously because the observation period was limited to 4 h. Our findings indicated that, by 4 h, MPs up to 3  $\mu\text{m}$  have the ability to penetrate the two barriers *in vivo*, albeit weakly. Our results provide the proof for mammals that NPs and MPs have the ability to penetrate the blood-brain and blood-testis barriers, which suggested that plastic pollution might be an important risk for human health.

There were three limitations to the present study. First, the observation period was short and the number of animals in each group was only three as a pilot study of toxicokinetics. We are planning to conduct a further study with a longer time course and a greater number of mice to confirm the conclusions drawn in this study. Second, MPs and NPs fibers are the most commonly form in environmental components; however, only PS beads were used in this study because of the lack of fibrous standards. It needs to be developed in the future for risk assessment of MPs and NPs pollution on human health. Third, only toxicokinetics for a single oral exposure were focused and the pathological mechanism of MPs and NPs had not been explored. More accurate evidences and their toxic effects even for a single exposure should be study further.

## CONCLUSION

In a conclusion, gavage of 100 nm, 3  $\mu\text{m}$ , and 10  $\mu\text{m}$  fluorescent PS beads in the present study provide the evidences on toxicokinetics of MPs and NPs in mammals *in vivo*. Our findings revealed that NPs can be rapidly absorbed into blood after a single oral exposure and accumulate in adipose tissues. NPs have the ability to penetrate the blood-brain and blood-testis barriers. The absorption and distribution of MPs were size-dependent. In comparison to NPs, MPs with diameter < 3  $\mu\text{m}$  could

be slowly absorbed into the blood and has the ability to invade the nervous system and reproductive system by 4 h after exposure.

## AUTHOR CONTRIBUTIONS

YANG Zuo Sen: Conceptualization, Methodology, Wring-original draft preparation, Funding Acquisition. BAI Ying Long and JIN Cui Hong: Methodology, Investigation, Wring-Review & Editing. NA Jun, ZHANG Rui, and GAO Yuan: Methodology, Investigation, Data curation. PAN Guo Wei: Conceptualization, Methodology, Wring-Review & Editing, Supervision. YAN Ling Jun: Conceptualization, Methodology, Wring-Review & Editing, Supervision, Funding Acquisition. SUN Wei: Conceptualization, Methodology, Investigation, Wring-Review & Editing, Project Administration.

## ACKNOWLEDGMENTS

We thank for the support from the Key Laboratory of Ministry of Education for TCM Viscera-State Theory and Applications, Liaoning University of Traditional Chinese Medicine and Dr. ZHANG Ze, SUI Guo Yuan and CHEN Li Juan for their technological guidance.

## ETHICS APPROVAL AND CONSENT TO PARTICIPATE

This study was conducted in accordance with the Declaration of Helsinki on ethical principles for medical research involving human subjects. The experimental protocol was approved by the Ethical Requirements of Experimental Animals of China Medical University (Number: CMU2019216).

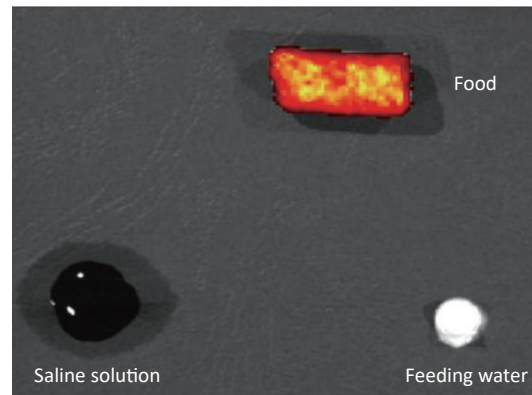
Received: January 5, 2022;

Accepted: June 13, 2022

## REFERENCES

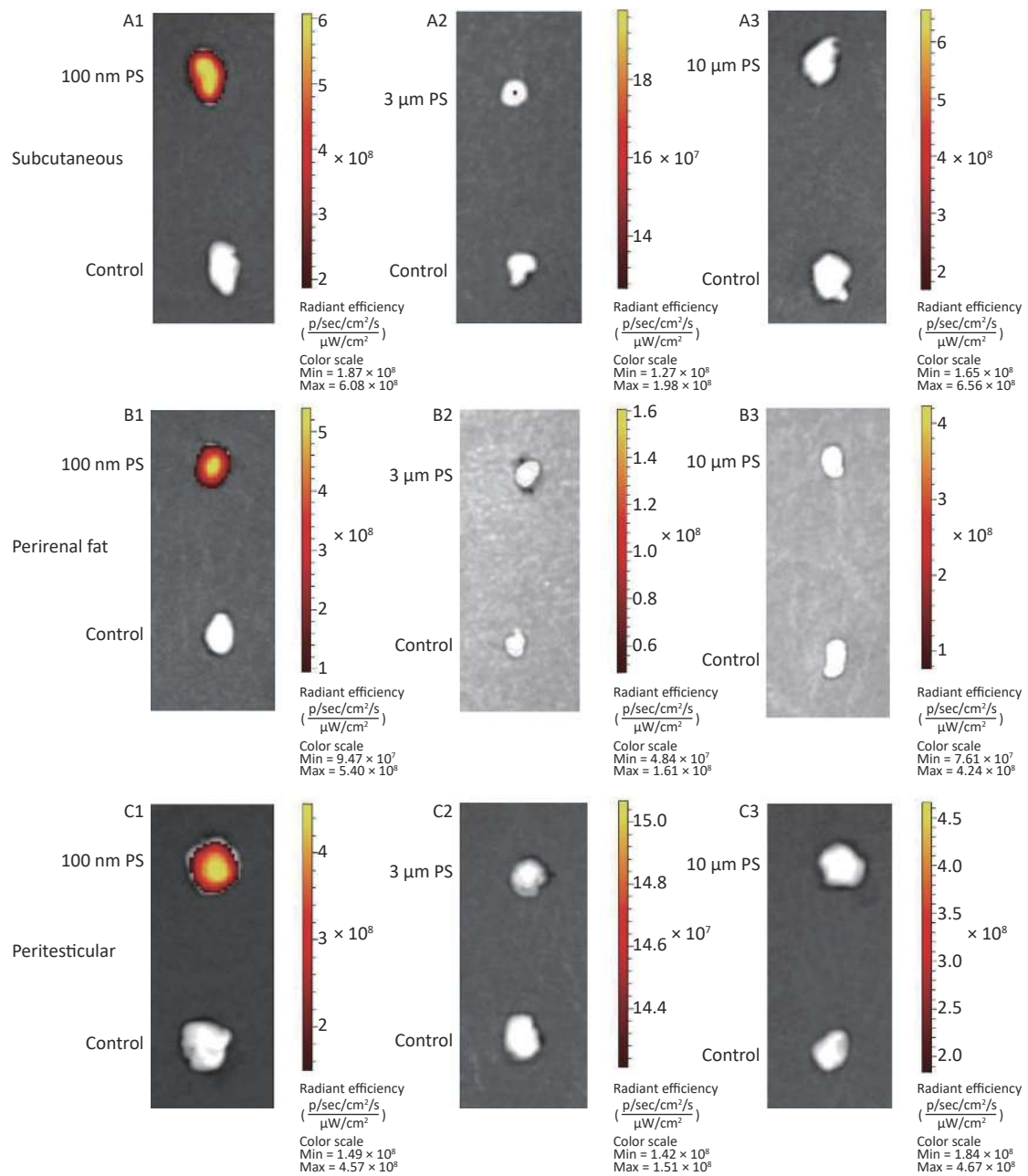
1. Plastics Europe. Plastics - the facts 2019 - an analysis of European plastics production, demand and waste data. <https://plasticseurope.org/wp-content/uploads/2021/10/2019-Plastics-the-facts.pdf>. [2022-10-26]
2. Lusher AL, Tirelli V, O'Connor I, et al. Microplastics in arctic polar waters: the first reported values of particles in surface and sub-surface samples. *Sci Rep*, 2015; 5, 14947.
3. Ivar do Sul JA, Costa MF, Barletta M, et al. Pelagic microplastics around an archipelago of the Equatorial Atlantic. *Mar Pollut Bull*, 2013; 75, 305–9.
4. Farrell P, Nelson K. Trophic level transfer of microplastic: *Mytilus edulis* (L.) to *Carcinus maenas* (L.). *Environ Pollut*, 2013; 177, 1–3.

5. Von Moos N, Burkhardt-Holm P, Köhler A. Uptake and effects of microplastics on cells and tissue of the blue mussel *Mytilus edulis* L. after an experimental exposure. *Environ Sci Technol*, 2012; 46, 11327–35.
6. Li JN, Yang DQ, Li L, et al. Microplastics in commercial bivalves from China. *Environ Pollut*, 2015; 207, 190–5.
7. Mathalon A, Hill P. Microplastic fibers in the intertidal ecosystem surrounding Halifax Harbor, Nova Scotia. *Mar Pollut Bull*, 2014; 81, 69–79.
8. Cox KD, Covernton GA, Davies HL, et al. Human consumption of microplastics. *Environ Sci Technol*, 2019; 53, 7068–74.
9. Kosuth M, Mason SA, Wattenberg EV. Anthropogenic contamination of tap water, beer, and sea salt. *PLoS One*, 2018; 13, e0194970.
10. Kutralam-Muniasamy G, Pérez-Guevara F, Elizalde-Martínez I, et al. Branded milks - are they immune from microplastics contamination? *Sci Total Environ*, 2020; 714, 136823.
11. Yang DQ, Shi HH, Li L, et al. Microplastic pollution in table salts from China. *Environ Sci Technol*, 2015; 49, 13622–7.
12. Guterres SS, Alves MP, Pohlmann AR. Polymeric nanoparticles, nanospheres and nanocapsules, for cutaneous applications. *Drug Target Insights*, 2007; 2, 147–57.
13. Fendall LS, Sewell MA. Contributing to marine pollution by washing your face: microplastics in facial cleansers. *Mar Pollut Bull*, 2009; 58, 1225–8.
14. Barría C, Brandts I, Tort L, et al. Effect of nanoplastics on fish health and performance: a review. *Mar Pollut Bull*, 2020; 151, 110791.
15. Jin YX, Lu L, Tu WQ, et al. Impacts of polystyrene microplastic on the gut barrier, microbiota and metabolism of mice. *Sci Total Environ*, 2019; 649, 308–17.
16. Lu L, Wan ZQ, Luo T, et al. Polystyrene microplastics induce gut microbiota dysbiosis and hepatic lipid metabolism disorder in mice. *Sci Total Environ*, 2018; 631–632, 449–58.
17. Deng YF, Zhang Y, Lemos B, et al. Tissue accumulation of microplastics in mice and biomarker responses suggest widespread health risks of exposure. *Sci Rep*, 2017; 7, 46687.
18. Xie XM, Deng T, Duan JF, et al. Exposure to polystyrene microplastics causes reproductive toxicity through oxidative stress and activation of the p38 MAPK signaling pathway. *Ecotoxicol Environ Saf*, 2020; 190, 110133.
19. Luo T, Zhang Y, Wang CY, et al. Maternal exposure to different sizes of polystyrene microplastics during gestation causes metabolic disorders in their offspring. *Environ Pollut*, 2019; 255, 113122.
20. Schirinzi GF, Pérez-Pomeda I, Sanchís J, et al. Cytotoxic effects of commonly used nanomaterials and microplastics on cerebral and epithelial human cells. *Environ Res*, 2017; 159, 579–87.
21. Wang FJ, Bexiga MG, Anguissola S, et al. Time resolved study of cell death mechanisms induced by amine-modified polystyrene nanoparticles. *Nanoscale*, 2013; 5, 10868–76.
22. Mattsson K, Johnson EV, Malmendal A, et al. Brain damage and behavioural disorders in fish induced by plastic nanoparticles delivered through the food chain. *Sci Rep*, 2017; 7, 11452.
23. EFSA panel on contaminants in the food chain (CONTAM). Presence of microplastics and nanoplastics in food, with particular focus on seafood. *EFSA J*, 2016; 14, e04501.
24. Jani P, Halbert GW, Langridge J, et al. Nanoparticle uptake by the rat gastrointestinal mucosa: quantitation and particle size dependency. *J Pharm Pharmacol*, 1990; 42, 821–6.
25. Stock V, Böhmert L, Lisicki E, et al. Uptake and effects of orally ingested polystyrene microplastic particles *in vitro* and *in vivo*. *Arch Toxicol*, 2019; 93, 1817–33.
26. Xu DH, Ma YH, Han XD, et al. Systematic toxicity evaluation of polystyrene nanoplastics on mice and molecular mechanism investigation about their internalization into Caco-2 cells. *J Hazard Mater*, 2021; 417, 126092.
27. Johnston H, Pojana G, Zuin S, et al. Engineered nanomaterial risk. Lessons learnt from completed nanotoxicology studies: potential solutions to current and future challenges. *Crit Rev Toxicol*, 2013; 43, 1–20.
28. Schür C, Rist S, Baun A, et al. When fluorescence is not a particle: the tissue translocation of microplastics in *Daphnia magna* seems an artifact. *Environ Toxicol Chem*, 2019; 38, 1495–503.
29. Cau A, Avio CG, Dessi C, et al. Benthic crustacean digestion can modulate the environmental fate of microplastics in the deep sea. *Environ Sci Technol*, 2020; 54, 4886–92.
30. Meng FF, Wang JP, Ping QN, et al. Quantitative assessment of nanoparticle biodistribution by fluorescence imaging, revisited. *ACS Nano*, 2018; 12, 6458–68.
31. Tartaro K, VanVolkenburg M, Wilkie D, et al. Development of a fluorescence-based *in vivo* phagocytosis assay to measure mononuclear phagocyte system function in the rat. *J Immunotoxicol*, 2015; 12, 239–46.
32. Kunda NK, Price DN, Muttill P. Respiratory tract deposition and distribution pattern of microparticles in mice using different pulmonary delivery techniques. *Vaccines (Basel)*, 2018; 6, 41.
33. McConnell EL, Basit AW, Murdan S. Measurements of rat and mouse gastrointestinal pH, fluid and lymphoid tissue, and implications for in-vivo experiments. *J Pharm Pharmacol*, 2008; 60, 63–70.
34. Lankveld DPK, Oomen AG, Krystek P, et al. The kinetics of the tissue distribution of silver nanoparticles of different sizes. *Biomaterials*, 2010; 31, 8350–61.
35. Li JY, Yu ZX, Han B, et al. Activation of the gpx4/tlr4 signaling pathway participates in the alleviation of selenium yeast on deltamethrin-provoked cerebrum injury in quails. *Mol Neurobiol*, 2022; 59, 2946–61.
36. Rossi G, Barnoud J, Monticelli L. Polystyrene nanoparticles perturb lipid membranes. *J Phys Chem Lett*, 2014; 5, 241–6.
37. Li SY, Han B, Wu PF, et al. Effect of inorganic mercury exposure on reproductive system of male mice: immunosuppression and fibrosis in testis. *Environ Toxicol*, 2022; 37, 69–78.

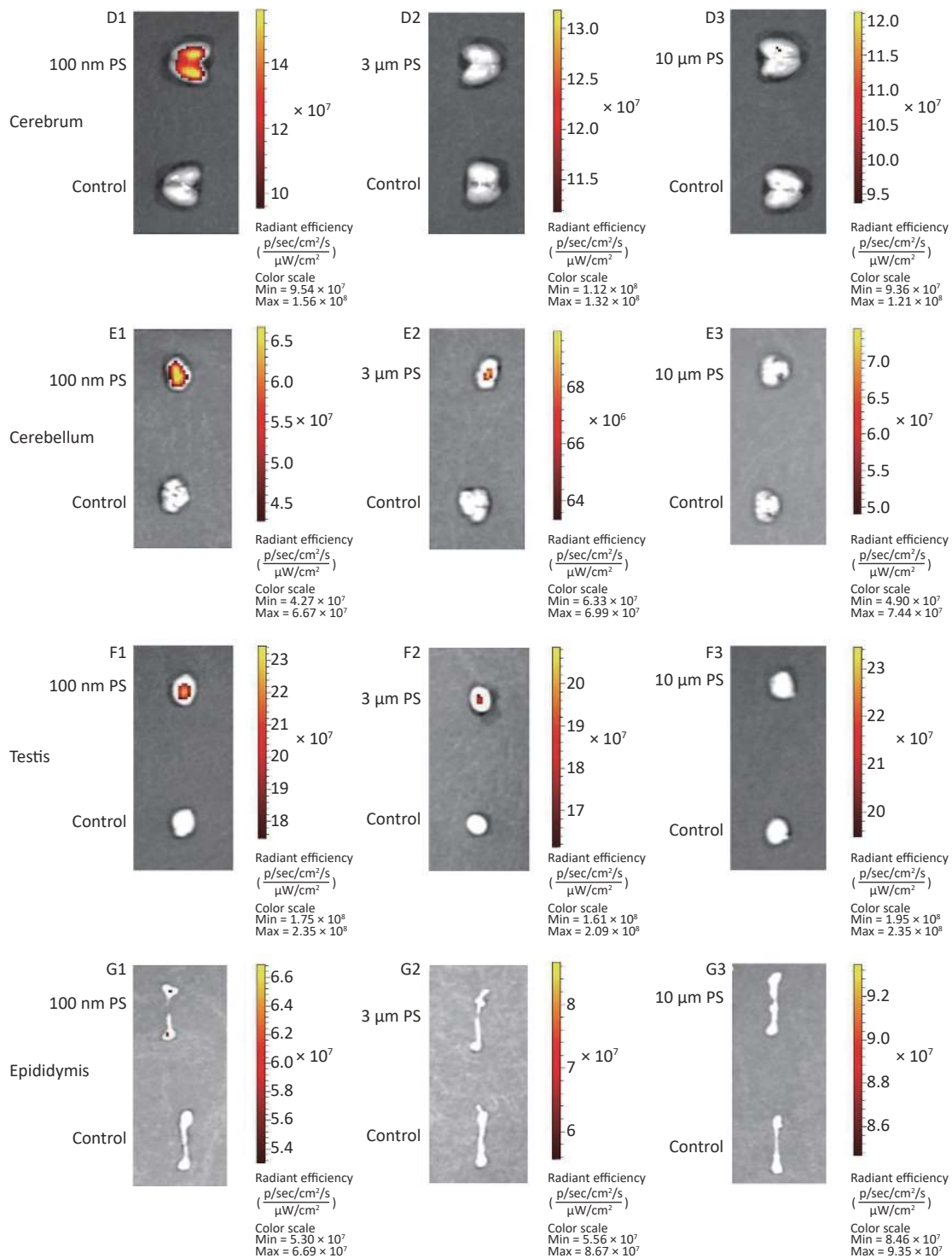


**Supplementary Figure S1.** The fluorescence image of food, 0.9% saline solution and feeding water by IVIS Spectrum.

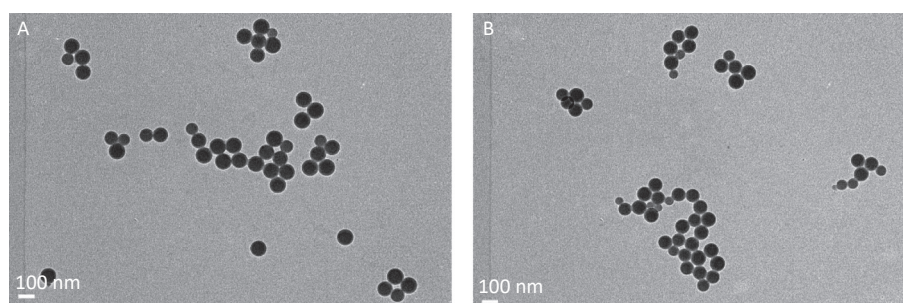




**Supplementary Figure S2-1.** The IVIS Spectrum small-animal imaging system images for the tissues examined.



**Supplementary Figure S2-2.** The IVIS Spectrum small-animal imaging system images for the tissues examined.



**Supplementary Figure S3.** The leaching examination by transmission electron microscope (10,000 $\times$ ). (A) is the image in dispersing condition of reversing gently group. (B) is the image of in dispersing condition of sonicating for 30 min group.